Fission-fragment angular distributions and excitation functions in fission following complete fusion and targetlike-fragment fission reactions of $^{19}F+^{232}Th$ at near- and sub-barrier energies

N. Majumdar and P. Bhattacharya
Saha Institute of Nuclear Physics, I/AF, Bidhannagar, Calcutta-700064, India

D. C. Biswas, R. K. Choudhury, D. M. Nadkarni, and A. Saxena
Nuclear Physics Division, BARC, Bombay-400085, India
(Received 1 July 1994; revised manuscript received 6 February 1995)

The fragment angular distribution and excitation functions of the fission following complete fusion (FFCF) have been measured after separating them from targetlike-fragment fission (TLFF) for the $^{19}F+^{232}Th$ system in the bombarding energy range of 84.5 to 106.5 MeV. The fraction of the targetlike-fragment fission was observed to increase with decreasing bombarding energy below the Coulomb barrier. The excitation function for fission following complete fusion reaction agrees well with coupled channel calculations. However, the $\langle l^2 \rangle$ values derived from the fragment anisotropy data of the FFCF events are found to be much larger than those calculated using the coupled channel transmission coefficient values. The discrepancy between the experimental and calculated $\langle l^2 \rangle$ values increases as the bombarding energy is decreased below the barrier.

PACS number(s): 25.70.Jj, 24.10.Eq

I. INTRODUCTION

Anomalous anisotropies in the angular distribution of fission fragments have been observed in several heavy-ion-induced nuclear reactions at near- and sub-barrier energies [1,2]. The fission-fragment anisotropy, i.e., $W(0°)/W(90°)$, is found to be larger than that predicted theoretically by the standard saddle-point statistical model (SSPSM) [3] for the fission of the compound nucleus formed by the fusion of the projectile and target nuclei. Several explanations have been forwarded to account for the discrepancies: invoking new aspects of reaction dynamics such as broadening of the l distribution at sub-barrier energies [2], and onset of new reaction channels such as fast fission, quasifission [4], and preequilibrium fission [5]. It is in this context that accurate measurement of fission-fragment anisotropies for fission following complete fusion (FFCF) events in heavy-ion reactions is of crucial importance.

At sub-barrier energies, FFCF cross sections fall very rapidly, and a dominant fraction of the fission events comes from the fission of a targetlike fragment (TLF) formed by direct noncompound processes such as transfer of a few nucleons from the projectile, nucleon exchange without a net transfer, or inelastic scattering. It is, therefore, necessary to take into account the contribution of the targetlike-fragment fission (TLFF) events to obtain the fission-fragment angular distributions of FFCF events for a proper comparison with the theoretical calculations. At present, there exist very little data on the fragment anisotropies, separately for fission following complete fusion and for targetlike-fragment fission, including transfer-induced fission events. Lestone *et al.* [6] have measured the fragment angular distributions of transfer-induced fission integrated over all the recoil angles for the $^{16}O+^{232}Th$ system at 86- and 90-MeV beam energies, which are found to have lower anisotropies $[W(0°)/W(90°) = 1.2$ and $1.3]$ as compared to the fission following complete fusion events.

In the present work, we have investigated the fission-fragment anisotropies for both FFCF and TLFF events for the $^{19}F+^{232}Th$ system at sub-barrier energies. Leigh *et al.* [7] have shown that in the $^{19}F+^{232}Th$ reaction at near- and sub-barrier energies, a large fraction of all fission events arise from targetlike-fragment fission. Earlier measurements of fission-fragment anisotropies reported by Zhang *et al.* [8] and Kailas *et al.* [9,10] correspond to all fission events, which are seen to be already anomalously large compared to the SSPSM predictions. Following the result of Lestone *et al.* [6] on the anisotropy of targetlike-fragment fission (TLFF) events, the elimination of the TLFF contribution is expected to result in further enhancement in fragment anisotropy for the fission following complete fusion (FFCF) events compared to that of all fission events. Recently Zhang *et al.* [11] have reported the measurements of angular distribution of fission fragments in fission following complete fusion reactions of $^{16}O+^{232}Th$, $^{19}F+^{232}Th$, and $^{16}O+^{238}U$ by employing the folding angle method to separate the FFCF from TLFF events. The authors, however, did not report the anisotropies and the fractions of targetlike fragment fission events that contribute at near- and sub-barrier energies in these reactions. They concluded that at sub-barrier energies anisotropies of the FFCF events are lower than that for all fission events, suggesting that the anisotropy of the TLFF events could be larger than that of the FFCF events, which is opposite to the results of Lestone *et al.* [6] for the $^{16}O+^{232}Th$ system. In our earlier work [12], we had reported that for the $^{19}F+^{232}Th$ reaction at 92.5-MeV bombarding energy the anisotropy

of fission following complete fusion is higher than the anisotropy for all fission events, which is again contrary to the results of Zhang *et al.* [11]. In order to examine afresh the anomalous behavior of the anisotropy of FFCF events in the $^{19}F+^{232}Th$ reaction, we report here the results on the study of the angular anisotropies and excitation functions for the fission following complete fusion (FFCF) and targetlike-fragment fission (TLFF) events at near- and sub-barrier energies.

In the present experiment, we have used the fission-fragment folding angle technique to measure the yields of FFCF and TLFF events as function of the fragment angle with respect to the beam direction. Since in the case of targetlike fragment fission there can be a large spread in the recoil angle of the TLF with respect to the direction of the beam, a proper analysis of the folding angle distribution requires a kinematic reconstruction of the momenta and angles of the recoils from the measured angular distributions of the projectilelike fragments (PLF). The analysis procedure adopted in the present work to separately determine the TLFF and FFCF yields is described briefly in the present paper, the details of which are being reported separately elsewhere [13]. In the present paper, we discuss the results obtained on the angular anisotropies of the fission following complete fusion after separating the contribution from the targetlike-fragment fission events and also the cross sections for these two types of fission events in the $^{19}F+^{232}Th$ reaction in bombarding energy range 84.5–106.5 MeV.

Section II describes the experimental details and data analysis procedure for obtaining the folding angle distributions and fitting of the experimental data to extract the FFCF and TLFF components. Section III contains the results and discussions on the fission-fragment anisotropies and excitation function of the FFCF events. Section IV contains the summary and conclusions of the present investigations.

II. EXPERIMENTAL PROCEDURE AND DATA ANALYSIS

The experiments were carried out using ^{19}F beams from the Bhabha Atomic Research Center-Tata Institute of Fundamental Research 14 UD Pelletron accelerator of Bombay. A self-supporting 1.8 mg cm^{-2} thick ^{232}Th target was used for the experiments. Two X-Y position-sensitive multistep avalanche counters of Breskin type [14] having active dimensions of 6.5 cm×5.0 cm and 15.0 cm×3.5 cm were used to detect the two fission fragments in coincidence. These position-sensitive detectors consist of an anode wire plane in the middle, two cathode wire-planes on either side of the anode, and X and Y sense wire planes interposed between the anode and the cathode wire planes. The detectors are operated typically at 2.5 torr of isobutane gas, and provide excellent timing, position sensitivity, and discrimination of the fission fragments from beamlike particles. The smaller detector was kept at 20.0 cm from the target, subtending an in-plane angle of about 18° at the target and was moved to cover laboratory angles of 10°–110° in overlapping steps. The longer detector was placed at a distance of 14.5 cm on the opposite side of the target covering about 60° in the reaction plane to detect the complementary fission fragments. A 300-μm-thick solid-state detector was placed in forward direction at 25° angle to monitor the elastically scattered ^{19}F ions. The monitor counts were used to normalize the angular distributions of fission fragments for different angular settings.

The position calibration of the fission-fragment detectors was achieved from the dips in the fragment yields in the detectors due to the shadows caused by the 0.6-mm-thick nylon wires used to support the thin windows of the detectors. The calibration was done using a ^{252}Cf source, mounted at the point of the target location. From the event-by-event information on the position of the two fission fragments in the two detectors, their angles of emission were calculated. The sum of the polar angles of emission of the complementary fission fragments were obtained for different angular bins (bin size of 2°) of the smaller detector. The azimuthal angle (ϕ) was restricted to about ±4°. Correction factors for the polar angle (θ) dependence of the solid angle and for the shadow of the nylon support wires were calculated and used to obtain the coincidence yields as a function of the folding angle of the fission fragments. The timing information from the two fission-fragment detectors was used to define the coincident fission events, and to reject any random coincidences in the data.

Figure 1 shows the folding angle distributions of the fragments for the $^{19}F+^{232}Th$ reaction at 92.5 MeV for some typical angular bins for fragments detected in the small detector. The components of targetlike-fragment fission (TLFF) and fission following complete fusion (FFCF) are seen distinctly in the data. The folding angle distribution for TLFF events at near- and sub-barrier

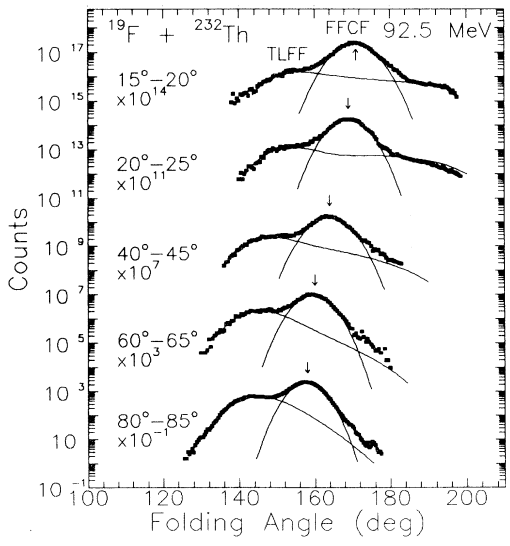

FIG. 1. Fission-fragment folding angle distributions (solid squares) at different laboratory angle for 5° bins of one of the fragments for FFCF and TLFF are shown. The arrows mark the positions of full momentum transfer. Simulations of the folding angle distributions for the TLFF and FFCF are shown by solid lines.

energies is expected to be much broader than that for FFCF events due to broad recoil angle distributions in the transfer reactions. Moreover, when the fixed detector angle is around one of the recoil directions, the folding angle distributions for the targetlike fragment fission splits into two components as expected from kinematic considerations. It may be noted that the earlier similar measurements by Zhang *et al.* [11] did not bring out these features, presumably because of the limited folding angle coverage in the geometry employed in their experiment. In order to extract the fission following complete fusion and targetlike fragment fission components from the folding angle data, we have simulated the shape of the folding angle distribution of the TLFF component from the results on the angular distributions of the projectilelike transfer reaction products. The angular distributions and energy spectra of the PLF's were measured in a separate experiment by using solid-state detector telescope [ΔE(17 μm)-E(500 μm)] at different laboratory angles. At sub-barrier energies, these angular distributions are seen to be broad and peaked at backward angles. These data were used for kinetic calculation of the energy and angular distribution of the recoiling nuclei, which are required to simulate the folding angle distribution of the targetlike-fragment fission events. Further details of the simulation procedure and data analysis are being reported separately [13]. The fission following complete fusion events are seen to peak at the folding angle expected for full momentum transfer, as calculations with the fragment energies using Viola's systematics [15] for symmetric mass split. The folding angle distributions were fitted by a Gaussian distribution to the FFCF component and the simulated Gaussian averaged shapes for the TLFF component. The areas of the simulated shape functions were kept as free parameters to fit the folding angle distribution data. The fits to the data are shown as the solid lines in Fig. 1. The position of the mean folding angle for fission following complete fusion (full momentum transfer) is marked by arrows. From the fits to the folding angle distributions, the laboratory angular distributions of the fission following complete fusion and targetlike-fragment fission components were extracted. Figure 2 shows the laboratory fragment angular distributions for all fission events, and for FFCF and TLFF events measured at different bombarding energies. In order to obtain the angular distributions in the center-of-mass frame, kinematic corrections are needed to be applied to the laboratory angular distributions for FFCF and TLFF data. The kinematic corrections for the FFCF events were carried out assuming full momentum transfer to the compound nucleus along the beam direction, and the average fragment velocities to correspond to energies given by Viola's systematics for symmetric mass split. In the case of the TLFF events, the center-of-mass correction depends on the velocity and angle of the recoils, which can in principle be calculated from the differential cross sections of projectilelike fragments. It was found that at a given laboratory angle there is a wide spread in the center-of-mass angle because of the large variation in the recoil directions and momenta of the recoiling nuclei undergoing fission. Thus an exact transformation of

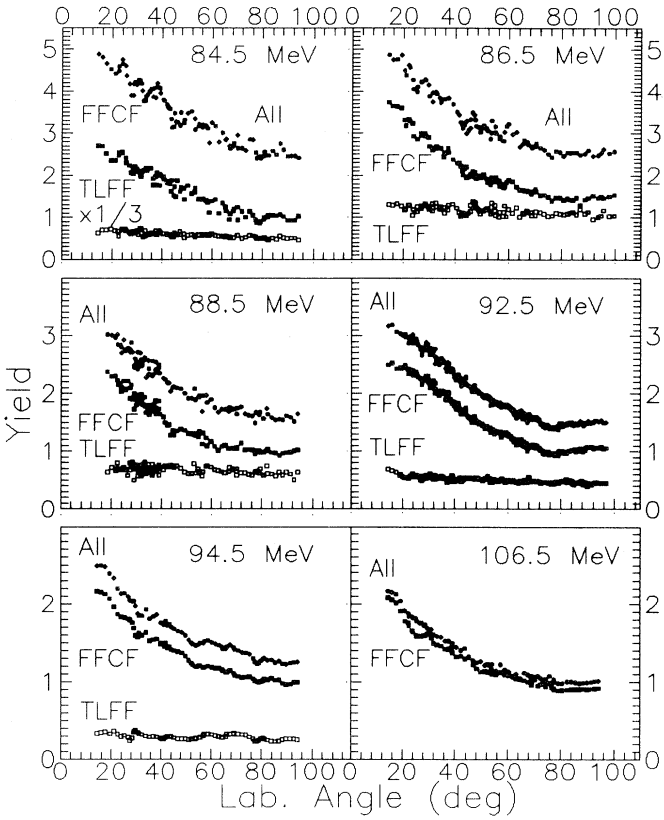

FIG. 2. Laboratory angular distributions for FFCF (solid squares), TLFF (open squares), and all fission events (solid circles) at different bombarding energies.

the angular distribution of TLFF events to the center-of-mass frame was not feasible, and we only report the angular anisotropies in the laboratory frame for these events. The center-of-mass angular distributions for the FFCF events were fitted with Legendre polynomials up to P_6 terms to obtain the angular anisotropies. We have seen that lower-order polynomial fits up to P_4 terms are not significantly different, and are within statistical errors of the data.

The excitation function for fission following complete fusion (FFCF) was obtained after correcting the FFCF yields for the measured angular distributions. We have normalized the cross sections of fission following complete fusion to the known value of the cross section measured at above barrier energy in earlier experiments [8,10], where the targetlike-fragment fission (TLFF) contributes a small fraction of all fission. The results on the excitation function and angular anisotropies are discussed in the next section.

III. RESULTS AND DISCUSSIONS

The fission-fragment angular distributions for fission following complete fusion (FFCF) can be theoretically calculated from the standard saddle-point statistical model (SSPSM) [16]. The angular distribution of the fis-

sion fragments for spinless target and projectile is given by

$$W(\theta) \propto \sum_{l=0}^{\infty}(2l+1)T_l \times \sum_{K=-l}^{l} \frac{(2l+1)|d^l_K(\theta)|^2 \exp(-K^2/2K_0^2)}{\sum_{K=-l}^{l}\exp(-K^2/2K_0^2)} . \quad (1)$$

Here, l is angular momentum of the fused nucleus, and K is its projection on the symmetry axis. T_l's are the transmission coefficients and $d^l_K(\theta)$'s are the usual d functions. The parameter K_0^2 is the variance of the truncated Gaussian distribution of K values, and is related to the effective moment of inertia J_{eff} and temperature T at the transition state, by

$$K_0^2 = J_{\text{eff}}T/\hbar^2 , \quad (2)$$

where

$$J_{\text{eff}}^{-1} = J_{\|}^{-1} - J_{\perp}^{-1} . \quad (3)$$

Here, $J_{\|}$ and $J_{\perp}$ refer to moments of inertia of the fissioning nucleus at the saddle point parallel and perpendicular to the symmetry axis, and are calculated from the finite range rotating liquid drop model of Sierk [17]. The temperature at the saddle point is determined from the relation

$$aT^2 = E^* - B_{\text{fiss}}(l) , \quad (4)$$

where E^* is the excitation energy at saddle point, which is calculated after correcting for prescission neutron emission, based on the experimental prescission neutron multiplicities of Hinde *et al.* [18] and by following the procedure of Rossner *et al.* [19] and Saxena *et al.* [20]. $B_{\text{fiss}}(l)$ is the l-dependent fission barrier, which is calculated adopting the procedure followed in [17]. The level density parameter a was taken to be $a = A/10$ as it describes light-heavy-ion-induced fission data better. At medium excitation energies, as in the present investigations, the angular anisotropy, $\alpha = W(0°)/W(90°)$, can be very well approximated by

$$\alpha = 1 + \langle l^2\rangle/4K_0^2 , \quad (5)$$

where $\langle l^2\rangle$ is the mean-square momentum of the fissioning nucleus.

The angular momentum distribution of the fissioning nucleus, which depends on the transmission coefficients T_l's as shown in Eq. (1), can be obtained from the coupled-channel calculations (CCDEF code) [21] by fitting the measured fission excitation functions. In the present calculations, we have assumed axially symmetric shapes of the target, characterized by nuclear quadrupole and hexadecapole deformation parameters $\beta_2 = 0.217$ and $\beta_4 = 0.09$. A nuclear potential $U_N(r, \theta_p, \theta_t)$ of Woods-Saxon type has been used:

$$U_N(r, \theta_p, \theta_t) = V_0\{1 - \exp\{[r - R(\theta_p, \theta_t)]/a_0\}\}^{-1} , \quad (6)$$

with $R = R_p + R_t + 0.29$ fm, $a_0 = 0.63$ fm, and $V_0 =$ 71.7 MeV. The subscripts (p, t) refer to the projectile and target, respectively. The following inelastic channels were included in the calculations: one of them being the 0.7744-MeV state of ^{232}Th with $\beta_3 = 0.09$ and others being 0.197-, 1.346-, 1.554-, and 2.780-MeV states of ^{19}F with $\beta_2 = 0.55$, $\beta_3 = 0.33$, $\beta_2 = 0.58$, and $\beta_4 = 0.22$, respectively.

The measured excitation function for the fission following complete fusion events is shown in Fig. 3. The results of Zhang *et al.* [11] have also been shown in the figure for the fission following complete fusion reaction. The solid line in the figure corresponds to the coupled-channel theory calculations, whereas the dashed line corresponds to calculations without coupling. The agreement between the experimental and the theoretical excitation functions with inclusion of channel coupling is quite satisfactory at all energies. At above barrier energies, the theoretical curve also explains the inclusive measurement of Leigh *et al.* [22] where the contribution of TLFF is small. We have extracted the transmission coefficients T_l's from the coupled-channel calculations and used these values to calculate the SSPSM predicted angular distribution.

Figure 4 shows typical experimental fragment angular distributions for fission following complete fusion (solid squares) at 92.5-MeV bombarding energy, along with the results of the theoretical (SSPSM) predictions (dashed line). It has been seen that the theoretical angular distributions are less anisotropic than the observed angular distributions. The angular anisotropies $[W(0°)/W(90°)]$ were obtained by fitting the angular distribution data with Legendre polynomials up to P_6 terms for both FFCF and all fission events. The center-of-mass angular distributions of all fission events were obtained by applying the same kinematic correction factors as that for FFCF events. The results for all fission events are also reported here to carry out a comparison with the earlier inclusive measurements where separation of FFCF and TLFF events was not carried out.

Figure 5(a) shows the results on the center-of-mass fission fragment anisotropies obtained for all fission events.

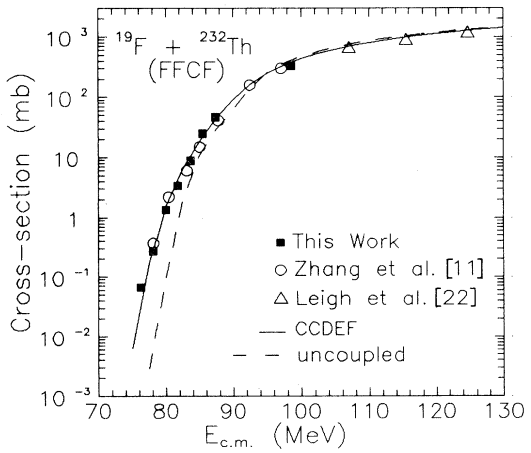

FIG. 3. The excitation function of fission following complete fusion for ^{19}F+^{232}Th. The CCDEF calculation is shown by solid line.

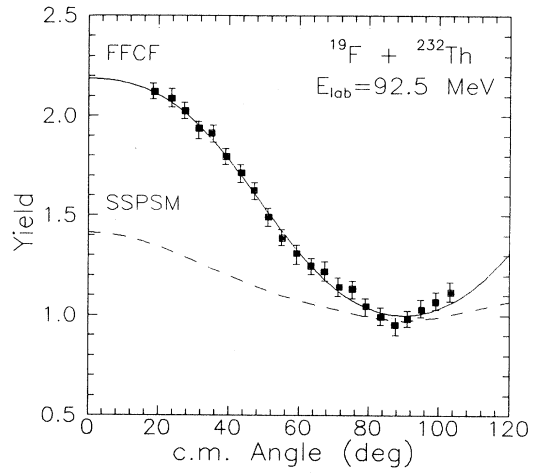

FIG. 4. Typical fragment angular distributions in the c.m. frame for FFCF at the bombarding energy of 92.5 MeV. The theoretical SSPSM angular distribution with prescission neutron emission correction is shown by the dashed line. The best fitted Legendre polynomial up to P_6 terms to the experimental data is shown by solid line.

Earlier results of Kailas *et al.* [9,10], Fujiwara *et al.* [23], and Zhang *et al.* [8] for all fission events are also shown in the figure for comparison. It is seen that the present result agrees with all the previous measurements except those of Zhang *et al.* [8]. The large anisotropies for all fission events reported by Zhang *et al.* [8] are not reproduced by our measurements. The bumplike increase in the anisotropy at $E_{c.m.} \sim 85$ MeV is also not borne out by the present work. In Fig. 5(b), we show the present results on the fragment anisotropies for the fission following complete fusion events along with the recent results of Zhang *et al.* [11]. It is seen that the two measurements agree with each other at all energies except at the lowest energy measured by Zhang *et al.* [11], where the anisotropy measured in the present experiment is somewhat higher than that of Zhang *et al.* [11]. The present measurements, however, extend to lower bombarding energies and the anisotropy is seen to be increasing with decreasing bombarding energy. As pointed out earlier, sub-barrier energies, the forward folding angle distributions become complex due to mixture of recoil angles and it is necessary to fit the full folding angle data with suitable shapes for both FFCF and TLFF components. Such a detailed fitting was not done by Zhang *et al.* [11], which might account for the discrepancy seen in the two measurements at sub-barrier energies. However, in both the measurements, the experimental fission fragment anisotropies for complete fusion events are seen to be much larger than the predictions of the standard saddle-point statistical model calculations, based on the rotating liquid drop model barrier parameters, and using the l distributions given by the coupled-channel calculations which fit the excitation function for FFCF events.

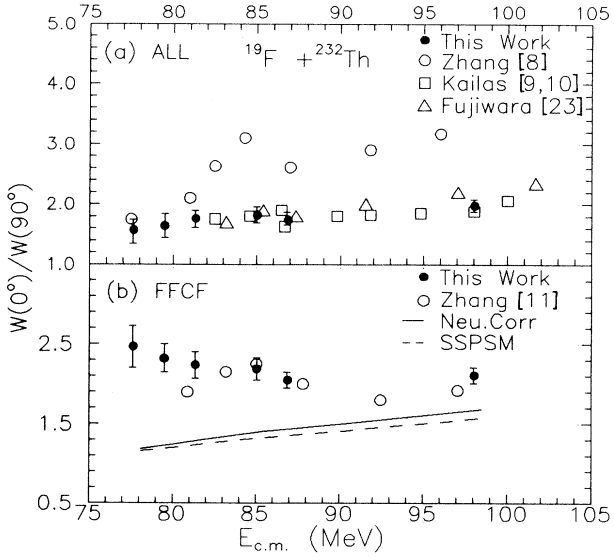

FIG. 5. The measured fragment anisotropies for (a) all fission events and (b) fission following complete fusion (FFCF) as a function of the c.m. energy of the projectile. The SSPSM calculations with (solid line) and without (dashed line) corrections for prescission neutron emissions are for comparison.

As pointed out earlier, in the statistical model formalism, the fission-fragment anisotropy is given by $\alpha = 1 + \langle l^2 \rangle / 4K_0^2$. The observed larger experimental anisotropy may imply either a larger value of $\langle l^2 \rangle$ or a smaller value of K_0^2 as compared to that given by theoretical models. Following the suggestion by Vandenbosch *et al.* [2], one may assume that the compound nuclear spin distribution gets broadened at sub-barrier energies, thereby leading to the observed discrepancy between the calculated and experimental values of the fission-fragment anisotropies. We have calculated the experimental $\langle l^2 \rangle$ values ($\langle l^2 \rangle_{ex}$), from the anisotropy data using the above equation and compared them with the $\langle l^2 \rangle_{theo}$ values given by the CCDEF calculations. Table I summarizes the present results on the experimental fragment anisotropy and the $\langle l^2 \rangle$ and the fusion cross sections (σ_{fus}) determined both experimentally and from theoretical CCDEF calculations. The results of calculations without channel coupling (corresponding to one-dimensional barrier penetration) have been also given in the table for comparison. As explained earlier, inclusion of channel coupling to the projectile and target deformations and to inelastic excitations improves the agreement between the calculated and experimental fusion cross sections to a large extent (see Fig. 3). At sub-barrier energies, the cross sections are enhanced by orders of magnitude with inclusion of channel coupling. However, the second moment of the spin distribution $\langle l^2 \rangle$ is still grossly underpredicted even with the inclusion of the deformation and inelastic excitations in the coupled channel calculations, as seen from the plot of $\langle l^2 \rangle$ with center-of-mass bombarding energy (Fig. 6). It is seen that at above-barrier energies, $\langle l^2 \rangle$ has a decreasing trend with decreasing bombarding energy, as expected from the calculations. However, at below-barrier energies, the experimental values are much too high and have an increasing tendency as the bombarding energy decreases. High anisotropy values at above barrier energies were explained earlier by Ramamurthy

TABLE I. Experimental and calculated parameters of fission-fragment angular distribution.

							Theory			
$E_{c.m.}$ (MeV)	α	J_{eff} (J_0^{-1})	T (MeV/nucl)	K_0^2	$\langle l^2\rangle_{ex}$ ($\hbar^2$)	σ_{fus}^{ex} (mb)	σ_{fus}^{un} (mb)	$\langle l^2\rangle_{fus}^{un}$ ($\hbar^2$)	σ_{fus}^{cou} (mb)	$\langle l^2\rangle^{cou}$ ($\hbar^2$)
98.44	2.11	1.77	1.17	289	1283	330.0	406.0	520	383.5	755
87.35	2.05	1.72	1.09	262	1100	46.8	28.3	87	42.9	377
85.50	2.19	1.72	1.06	254	1209	25.0	13.9	87	22.6	341
81.80	2.24	1.71	1.04	248	1230	3.4	0.94	87	4.7	236
79.95	2.32	1.70	1.03	244	1288	1.4	0.087	87	1.5	182
78.10	2.47	1.69	1.01	238	1399	0.3	0.006	87	0.32	134

et al. [5] to be due to a small admixture of a new class of events called "preequilibrium fission" which takes place for the systems having entrance channel mass asymmetry $\alpha_A = (A_T - A_P)/(A_T + A_P)$ less than the critical Businaro-Gallone mass asymmetry (α_{crit}^{BG}). Preequilibrium fission events are characterized by a narrow K distribution at the fission saddle point, thereby having very large anisotropies as compared to the normal fission events. According to the preequilibrium fission model [5], the probability of preequilibrium increases with the excitation energy of the system. Hence at lower bombarding energies, the contribution of preequilibrium fission events is expected to be less. The present observation of increasing anomaly in fragment anisotropy at subbarrier energies cannot be understood in the framework of the preequilibrium fission model. Moreover, the subbarrier anomaly in the fragment anisotropy is observed for a large number of systems which have entrance channel mass asymmetry on either side of the liquid drop Businaro-Gallone mass asymmetry. An alternative explanation of larger fragment anisotropy is ascribable to a broadening of the fusion l distribution at sub-barrier energies as suggested by Vandenbosch *et al.* [2]. We have seen that the CCDEF calculations with inclusion of deformation and inelastic excitation of the target and projectiles do give rise to certain broadening of the l distribution as shown in Fig. 6. However, the theoretical calculations still grossly underpredict the second moment of the spin distribution. It is still to be seen whether incorporating nucleon and cluster transfer channels in the CCDEF calculations can explain the present results. It may be noted that some recent coupled reaction channel calculations do predict large broadening in the l distribution due to coupling of Coulomb excitations and transfer channels in certain systems [24]. We also notice that the fraction of transfer-induced fission to compound nucleus fission has a similar increasing trend as the fragment anisotropy, indicating certain possible link of the anomalous behavior with the nucleon transfer process.

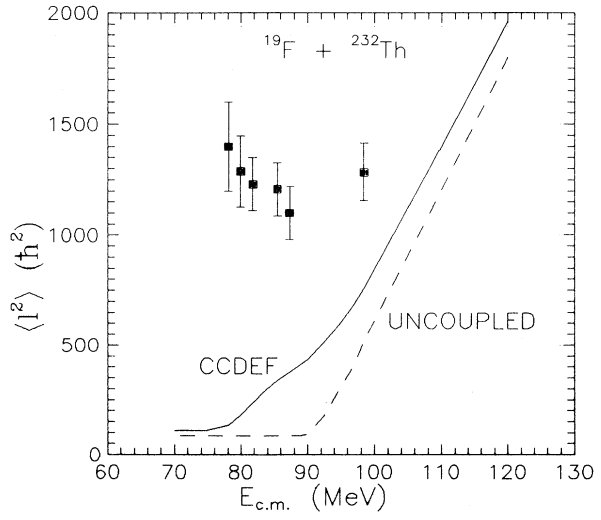

FIG. 6. Comparison of the experimental and calculated $\langle l^2\rangle$ values as a function of the center-of-mass projectile energy with (solid line) and without channel coupling (dashed line).

IV. SUMMARY AND CONCLUSIONS

In the present work, we report the fragment anisotropies in fission following complete fusion and targetlike-fragment fission components at near- and subbarrier energies in the $^{19}F+^{232}Th$ reactions. It is found that the fragments arising from fission following complete fusion have larger angular anisotropies as compared to the inclusive all fission events. The laboratory anisotropy of the targetlike-fragment fission events is of the order of 1.2–1.3 at all the energies measured in the present work. The center-of-mass anisotropy of the FFCF events are found to be larger than that expected from SSPSM calculations. The $\langle l^2\rangle_{ex}$ values derived from fragment anisotropy data are also much larger than those given by the CCDEF calculations at sub-barrier energies. The broadening of the l distributions at sub-barrier energies can possibly arise due to strong coupling of certain transfer and Coulomb excitation channels to the fusion reactions which have not been incorporated in the CCDEF calculations. Measurement of fragment anisotropies for more systems at sub-barrier energies is necessary for a systematic understanding of the behavior of l distributions at below-barrier energies.

ACKNOWLEDGMENTS

The authors are thankful to Dr. S. S. Kapoor for many useful discussions. We also acknowledge the help of the operating staff of the pelletron accelerator at Bombay.

[1] L. C. Vaz and J. M. Alexander, Phys. Rep. **97**, 1 (1983).
[2] R. Vandenbosch, T. Murakami, C.-C. Sahm, D. D. Leach, A. Ray, and M. J. Murphy, Phys. Rev. Lett. **56**, 1234 (1986).
[3] I. Halpern and V. M. Strutinsky, *Proceedings of the 2nd United Nations International Conference on Peaceful Uses of Atomic Energy*, Geneva (United Nations Publication, Geneva, 1958), Vol. 15, p. 408.
[4] B. B. Back, R. R. Betts, J. E. Gindler, B. D. Wilkins, S. Saini, M. B. Tsang, C. K. Gelbke, W. G. Lynch, M. A. Mcmahan, and P. A. Baisden, Phys. Rev. C **32**, 195 (1985).
[5] V. S. Ramamurthy and S. S. Kapoor, Phys. Rev. Lett. **54**, 178 (1985); V. S. Ramamurthy *et al.*, *ibid.* **65**, 25 (1990).
[6] J. P. Lestone, J. R. Leigh, J. O. Newton, and J. X. Wei, Nucl. Phys. **A509**, 178 (1990).
[7] J. R. Leigh, R. M. Diamond, A. Johnston, J. O. Newton, and S. H. Sie, Phys. Rev. Lett. **42**, 153 (1979).
[8] Huanqiao Zhang, Zuhua Liu, Jincheng Xu, Ming Ruan, and Kan Xu, Nucl. Phys. **A538**, 229c (1992).
[9] S. Kailas *et al.*, Phys. Rev. C **43**, 1466 (1991).
[10] S. Kailas, A. Navin, A. Chatterjee, P. Singh, A. Saxena, D. M. Nadkarni, D. C. Biswas, R. K. Choudhury, and S. S. Kapoor, Pramana J. Phys. **41**, 339 (1993).
[11] Huanqiao Zhang, Zuhua Liu, Jincheng Xu, Xing Qian, Yu Qiao, Chengjian Lin, and Kan Xu, Phys. Rev. C **49**, 926 (1994).
[12] P. Bhattacharya, D. C. Biawas, P. Basu, A. Saxena, S. Bhattacharya, V. S. Ambekar, R. K. Choudhury, M. L. Chatterjee, and D. M. Nadkarni, Proc. DAE NP Symp. **35B**, 192 (1992).
[13] P. Bhattacharya, N. Majumdar, P. Basu, M. L. Chatterjee, D. C. Biswas, A. Saxena, V. S. Ambekar, R. K. Choudhury, and D. M. Nadkarni, Nuovo Cimento (to be published).
[14] A. Breskin, Nucl. Instrum. Methods **196**, 11 (1982).
[15] V. E. Viola, K. Kwiatowski, and M. Walker, Phys. Rev. C **31**, 1550 (1985).
[16] R. Vandenbosch and J. R. Huizenga, *Nuclear Fission* (Academic, New York, 1973), p. 183.
[17] A. J. Sierk, Phys. Rev. C **33**, 2039 (1986).
[18] D. J. Hinde, H. Ogata, M. Tanaka, T. Shimoda, N. Takahashi, A. Shinohara, S. Wakamatsu, K. Katori, and H. Okamura, Phys. Rev. C **39**, 2268 (1989).
[19] H. Rossner, D. J. Hinde, J. R. Leigh, J. P. Lestone, J. O. Newton, J. X. Wei, and S. Elfstrom, Phys. Rev. C **45**, 419 (1992).
[20] A. Saxena, S. Kailas, A. Karnick, and S. S. Kapoor, Phys. Rev. C **47**, 403 (1993).
[21] J. Fernandez-Neillo, C. H. Dasso, and S. Landowne, Comput. Phys. Commun. **54**, 409 (1989).
[22] J. R. Leigh, cross sections as reported in Zhang *et al.* [Nucl Phys. **A538**, 229c (1992)].
[23] H. Fujiwara, S. C. Jeong, Y. H. Pu, T. Mizota, H. Kugoh, Y. Futami, Y. Nagashima, and S. M. Lee, University of Tsukuba Report (unpublished).
[24] I. J. Thomson, M. A. Nagarajan, J. S. Lilley, and M. J. Smithson, Nucl. Phys. **A505**, 84 (1989).